The Astrophysical Journal, 893:36 (14pp), 2020 April 10 https://doi.org/10.3847/1538-4357/ab7eb4

Reinflation of Warm and Hot Jupiters

Thaddeus D. Komacek[1], Daniel P. Thorngren[2], Eric D. Lopez[3,4], and Sivan Ginzburg[5]
[1] Department of the Geophysical Sciences, The University of Chicago, Chicago, IL 60637, USA; tkomacek@uchicago.edu
[2] Institute for Research on Exoplanets, Université de Montréal, Montréal, Québec, H3T 1J4, Canada
[3] NASA Goddard Space Flight Center, Greenbelt, MD 20771, USA
[4] GSFC Sellers Exoplanet Environments Collaboration, USA
[5] Department of Astronomy, University of California at Berkeley, CA 94720-3411, USA
Received 2020 February 5; revised 2020 March 3; accepted 2020 March 9; published 2020 April 14

Abstract

Understanding the anomalous radii of many transiting hot gas-giant planets is a fundamental problem of planetary science. Recent detections of reinflated warm Jupiters orbiting post-main-sequence stars and the reinflation of hot Jupiters while their host stars evolve on the main sequence may help constrain models for the anomalous radii of hot Jupiters. In this work, we present evolution models studying the reinflation of gas giants to determine how varying the depth and intensity of deposited heating affects both main-sequence reinflation of hot Jupiters and post-main-sequence reinflation of warm Jupiters. We find that deeper heating is required to reinflate hot Jupiters than is needed to suppress their cooling, and that the timescale of reinflation decreases with increasing heating rate and depth. We find a strong degeneracy between heating rate and depth, with either strong shallow heating or weak deep heating providing an explanation for main-sequence reinflation of hot Jupiters. This degeneracy between heating rate and depth can be broken in the case of post-main-sequence reinflation of warm Jupiters, as the inflation must be rapid to occur within post-main-sequence evolution timescales. We also show that the dependence of heating rate on the incident stellar flux inferred from the sample of hot Jupiters can explain reinflation of both warm and hot Jupiters. TESS will obtain a large sample of warm Jupiters orbiting post-main-sequence stars, which will help to constrain the mechanism(s) causing the anomalous radii of gas-giant planets.

Unified Astronomy Thesaurus concepts: Exoplanet evolution (491); Extrasolar gas giants (509); Hot Jupiters (753); Planetary interior (1248); Stellar evolution (1599); Planetary structure (1256)

1. Introduction

The observation that many transiting hot Jupiters have radii larger than expected from standard evolutionary models is an outstanding question of exoplanetary science (Guillot & Showman 2002; Baraffe et al. 2010, 2014; Fortney et al. 2010; Laughlin & Lissauer 2015; Laughlin 2018). A variety of mechanisms have been proposed to explain the anomalous transit radii of hot Jupiters (Weiss et al. 2013; Baraffe et al. 2014), including tidal mechanisms (Bodenheimer et al. 2001; Gu et al. 2003, 2004, 2019; Jackson et al. 2008; Ibgui & Burrows 2009; Miller et al. 2009; Arras & Socrates 2010; Ibgui et al. 2010; Leconte et al. 2010), modifications to the microphysics of hot Jupiters (Burrows et al. 2007; Chabrier & Baraffe 2007; Leconte & Chabrier 2012; Kurokawa & Inutsuka 2015), incident stellar-flux-driven hydrodynamic mechanisms (Guillot & Showman 2002; Showman & Guillot 2002; Youdin & Mitchell 2010; Tremblin et al. 2017; Sainsbury-Martinez et al. 2019), and ohmic dissipation (Batygin & Stevenson 2010; Perna et al. 2010; Batygin et al. 2011; Huang & Cumming 2012; Menou 2012; Rauscher & Menou 2013; Wu & Lithwick 2013; Rogers & Komacek 2014; Rogers & Showman 2014; Ginzburg & Sari 2016). Studies of the radius distribution of hot Jupiters (Demory & Seager 2011; Laughlin et al. 2011; Miller & Fortney 2011; Thorngren & Fortney 2018) have shown that radius anomalies only occur for gas giants with equilibrium temperatures in excess of 1000 K. Additionally, Laughlin et al. (2011), Weiss et al. (2013), and Thorngren & Fortney (2018) showed that the radii of hot Jupiters correlate with incident flux. As a result, the mechanism that inflates hot Jupiters is directly tied to the incident flux from the host star. Recently, Thorngren & Fortney (2018) found that the fraction of irradiation that is converted to deposited heat must peak at an intermediate equilibrium temperature of $\sim$1600 K and fall off for both hotter and colder planets.

Lopez & Fortney (2016) predicted that warm Jupiters will reinflate if their equilibrium temperature crosses the 1000 K heating threshold as their host stars evolve, provided that sufficient heat is deposited deep within the planet. Recent K2 observations of warm Jupiters orbiting post-main-sequence stars have found three candidate reinflated planets (Grunblatt et al. 2016, 2017, 2019). All of these planets have significantly inflated radii of $\approx$1.3–1.45 $R_{\rm Jup}$, which can be explained by heating at the very center of the planet with a deposited heating rate that is $\approx$0.03% of the incident stellar power (Grunblatt et al. 2017). Hartman et al. (2016) found evidence that hot Jupiters reinflate while their host stars brighten during main-sequence evolution. Main-sequence reinflation requires deposited heat, as mechanisms that only slow interior cooling cannot cause an increase in the planetary radius over time. D. Thorngren et al. (2020, in preparation) confirmed the finding of main-sequence reinflation using a Bayesian structural analysis of 232 hot Jupiters, finding evidence for a correlation between planetary radius and fractional age (age normalized by the main-sequence lifetime) of the host star. Additionally, D. Thorngren et al. (2020, in preparation) found that the radii of hot Jupiters track the incident flux from their host stars, not the age of the star. These observations of both main-sequence and post-main-sequence reinflation show that the incident stellar flux and deposited heating rates are linked—if the deposited heating rate were constant, the radius of the planet would either decrease or stay constant over time.

Lopez & Fortney (2016) found that reinflation can occur in the limiting case of heat that is deposited at the center of the planet. However, studies using heating profiles relevant for individual dissipation mechanisms differ on whether shallower heating can reinflate hot Jupiters. Batygin et al. (2011) found that ohmic dissipation can cause reinflation of hot Jupiters, while Wu & Lithwick (2013) and Ginzburg & Sari (2016) found that ohmic dissipation can only stall contraction, not lead to significant reinflation. This is because heating reinflates planets from the heating level downward, and the timescale for deposited heating to warm up the interior of the planet scales inversely with the heating depth (Ginzburg & Sari 2016). For ohmic dissipation, Ginzburg & Sari (2016) found that the timescale for reinflation is $\sim$30 Gyr, much longer than the $\sim$1 Gyr cooling timescale. A key difference between the numerical models of Batygin et al. (2011) and Wu & Lithwick (2013) is that Batygin et al. (2011) include the increase in incident stellar power with increasing planetary radius while Wu & Lithwick (2013) do not. For a fixed conversion rate of incident stellar power to energy deposition, this leads to an increase in the deposited heat with increasing planetary radius. In this paper, we will show that including this feedback between the planetary radius, incident stellar power, and heating rate can enhance reinflated planet radii.

The constraints derived by Thorngren & Fortney (2018) on the heating rate needed to explain the sample of inflated hot Jupiters assume that the heat is deposited at the very center of the planet. However, Spiegel & Burrows (2013), Ginzburg & Sari (2015), and Komacek & Youdin (2017) showed that there is a degeneracy between the heating rate and the depth of heating—deeper heating requires weaker heating rates to lead to a given radius, and vice versa. Observations of reinflated warm Jupiters orbiting post-main-sequence stars provide an avenue in which this degeneracy can be broken. This is because the reinflation timescale is strongly dependent on the depth of heating (Ginzburg & Sari 2016), which is dependent on the heating mechanism. Because post-main-sequence evolution timescales are fast ($\sim$100 Myr), only sufficiently deep heating will lead to post-main-sequence reinflation of warm Jupiters.

In this paper, we study both the reinflation of hot Jupiters while their host stars evolve on the main sequence (which we term "main-sequence reinflation") and the reinflation of warm Jupiters while their host stars evolve on the post-main sequence (termed "post-main-sequence reinflation"). This work builds off of that of Lopez & Fortney (2016) and uses a similar methodology to Komacek & Youdin (2017). We improve on previous work by studying how varying both heating rate and depth affects reinflation. Additionally, we study both main-sequence and post-main-sequence reinflation with a unified framework. Lastly, we show how the degeneracy between heating rate and heating depth can be broken with future observations of reinflated gas giants.

This paper is organized as follows. In Section 2, we describe our model setup and each of our three simulation grids studying reinflation. The results of these numerical experiments are shown in Section 3. We develop an analytic theory for reinflation due to point-source energy deposition in Section 4 and compare our theory to the results of our numerical experiments. We discuss our results and describe how observations of reinflation can test inflation mechanisms in Section 5, and conclude in Section 6.

2. Methods

2.1. Numerical Model

In this work, we use the MESA stellar and planetary evolution code (Paxton et al. 2011, 2013, 2015, 2018, 2019) to solve the time-dependent equations of stellar structure (Chandrasekhar 1939; Kippenhahn et al. 2012) applied to gas-giant planets. Our modeling framework is one-dimensional (1D), and as a result does not take into account either changes in the planetary structure as a function of latitude and longitude or atmospheric dynamics that can act to transport heat, limitations that are both described in further detail below. The planetary structure equations we solve include the mass conservation equation,

$$\frac{dm}{dr} = 4\pi r^2 \rho, \tag{1}$$

where m is the enclosed mass at a radius r, with mass density ρ. We ensure hydrostatic equilibrium,

$$\frac{dP}{dm} = -\frac{Gm}{4\pi r^4}, \tag{2}$$

where P is the pressure and G is the gravitational constant. Energy conservation is included as

$$\frac{dL}{dm} = \epsilon_{\rm grav} + \epsilon_{\rm irr} + \epsilon_{\rm dep}, \tag{3}$$

where L is the outgoing luminosity, $\epsilon_{\rm grav} = -TdS/dt$ (where T is temperature) is the loss or gain of entropy (S) due to gravitational contraction or inflation, $\epsilon_{\rm irr}$ is additional heating due to irradiation, and $\epsilon_{\rm dep}$ represents internal heat deposition. We describe our choices for $\epsilon_{\rm irr}$ and $\epsilon_{\rm dep}$ in further detail below. Lastly, we solve the energy transport equation,

$$\frac{dT}{dm} = -\frac{GmT}{4\pi r^4 P}\nabla, \tag{4}$$

where $\nabla \equiv d\ln T/d\ln P$ is the logarithmic temperature gradient, set equal to the smaller of the adiabatic gradient $\nabla_{\rm ad}$ or radiative gradient $\nabla_{\rm rad}$. In radiative regions, the temperature gradient is set equal to the radiative gradient

$$\nabla_{\rm rad} = \frac{3}{64\pi\sigma G}\frac{\kappa L P}{m T^4}, \tag{5}$$

where σ is the Stefan–Boltzmann constant and κ is the opacity, updated from Freedman et al. (2008) as described in Paxton et al. (2013) and assuming a dust-free solar composition. We use a zero-width radiative–convective boundary and do not model convective overshoot, which would cause the exchange of energy in both directions across the radiative–convective boundary (Youdin & Mitchell 2010; Leconte & Chabrier 2012). Additionally, our use of a 1D modeling framework does not consider the possibility that the radiative–convective boundary is nonuniform (Budaj et al. 2012; Rauscher & Showman 2014). Equations (1)–(4) are closed using the MESA equation of state (Paxton et al. 2019), which is largely from Saumon et al. (1995) for the temperatures and densities relevant for gas-giant planets.

We use the same basic model setup as Komacek & Youdin (2017), studying gas giants that are both externally irradiated and have deposited heating in their atmospheres or interiors.

However, instead of studying how heating slows the radius contraction of hot Jupiters as in Komacek & Youdin (2017), in this work we study the reinflation of both warm and hot Jupiters. We study reinflation using three separate model grids: an idealized suite studying the process by which reinflation occurs, a suite of models studying reinflation of hot Jupiters during main-sequence evolution of their host stars, and a suite studying the reinflation of warm Jupiters orbiting post-main-sequence stars. These model grids are described in detail in Section 2.2.

We incorporate irradiation and deposited heating by adding extra energy terms $\epsilon_{\rm irr}$ and $\epsilon_{\rm dep}$ to the energy conservation equation, as in Komacek & Youdin (2017). The incoming stellar flux $F_\star$ is incorporated as an energy generation rate,

$$\epsilon_{\rm irr} = \frac{F_\star}{4\Sigma_p}, \tag{6}$$

applied in an outer mass column Σ_p of the planet as in Valsecchi et al. (2015), Owen & Wu (2016), and Komacek & Youdin (2017). We describe our choices for Σ_p in Section 2.2. This irradiation leads to a slight increase in the radius relative to non-irradiated models, but when implemented in 1D structure models cannot explain the radius inflation of many hot Jupiters (Arras & Bildsten 2006; Fortney et al. 2007). Irradiation powers atmospheric circulation that acts to transport heat both from day to night (Perez-Becker & Showman 2013; Komacek & Showman 2016; Komacek et al. 2017) and vertically (Youdin & Mitchell 2010; Tremblin et al. 2017; Zhang & Showman 2018; Komacek et al. 2019; Sainsbury-Martinez et al. 2019), but this is not included in our modeling framework.

We model deposited heating as an additional term in the extra energy dissipation rate $\epsilon_{\rm extra}$, as was done in previous studies of gaseous planet evolution with MESA (Wu & Lithwick 2013; Komacek & Youdin 2017; Millholland 2019). This framework models direct heat deposition and does not take into account heat transport by, e.g., the deep atmospheric circulation (Sainsbury-Martinez et al. 2019). The heating rate $\epsilon_{\rm dep}$ is set to be Gaussian in pressure, with a standard deviation of half of a pressure scale height, as in Komacek & Youdin (2017). We consider a range of integrated heating rates,

$$\Gamma = \int_0^{M_p} \epsilon_{\rm dep} dm, \tag{7}$$

where M_p is the mass of the planet. We set the integrated heating rates to different fractions of the incident stellar power as

$$\gamma = \frac{\Gamma}{L_{\rm irr}}, \tag{8}$$

where the incident stellar power is

$$L_{\rm irr} = \pi R_p^2 F_\star, \tag{9}$$

with R_p the radius of the planet at the photosphere, where the optical depth to incoming radiation $\tau = 2/3$. We vary γ between 10^{-5} and 0.1 in all of our simulation grids. We consider heating centered at deposition pressures $P_{\rm dep}$ ranging from 1 to 10^6 bars and include cases with heating at the very center of the planet.

For all of our simulations, we use an initial model of an HD 209458b analog with a mass of 0.69 $M_{\rm Jup}$, a composition with a helium fraction $Y = 0.24$, metallicity $Z = 0.02$, and without a heavy-element core as in the HD 209458b models of Guillot & Showman (2002) and Komacek & Youdin (2017). The stopping points of our simulations are different for each model grid, as described in the following Section 2.2.

2.2. Simulation Grids

We conduct three separate grids of MESA simulations to study the reinflation of gas giants, as described below.

2.2.1. Reinflation of an Evolved Hot Jupiter

Our first suite of models studies the reinflation of an evolved hot Jupiter that undergoes fixed rates of irradiation and deposited heating. These simulations are idealized and do not directly apply to either the case of main-sequence reinflation of hot Jupiters or post-main-sequence reinflation of warm Jupiters. However, they are useful for understanding the process by which planets reinflate, and we compare the results from this suite of numerical experiments to analytic theory in Section 4. The starting point for these simulations is an HD 209458b model which has been evolved for 10 Gyr without any deposited heating, with a final radius of $1.08 R_{\rm Jup}$. We then reinflate the planet for 10 Gyr including deposited heating with varying heating rate and depth.

In this suite of simulations, we keep the incident stellar flux fixed at $F_\star = 1.0012 \times 10^9$ erg cm^{-2} s^{-1}, which corresponds to a full-redistribution equilibrium temperature of $T_{\rm eq} = 1450$ K. The outer mass column in which irradiation is applied is also fixed at $\Sigma_p = 250$ g cm^{-2}. Our chosen Σ_p is equal to a visible opacity of $\kappa_{\rm vis} = 4 \times 10^{-3}$cm^2 g^{-1}, as used in Fortney et al. (2008), Guillot (2010), and Owen & Wu (2016). For this visible opacity, the $\tau = 1$ level to incoming irradiation lies at a pressure of 0.23 bars for the present-day radius of HD 209458b. These values of incident stellar flux and irradiated column mass are the same as those used in Komacek & Youdin (2017). Additionally, in this suite of simulations, we keep the heating rate fixed in time and do not include the increase in the heating rate due to the increasing planetary cross-sectional area. Instead, as in Komacek & Youdin (2017), the heating rate is kept to a fixed fraction of the present-day incident stellar power of HD 209458b, which is 2.4×10^{29} erg s^{-1}. This model suite can hence be considered as the planetary reheating analog to the simulations of Komacek & Youdin (2017), who studied how heating can slow planetary cooling. We describe the results from this simulation grid and directly compare to the results of Komacek & Youdin (2017) in Section 3.1.

2.2.2. Main-sequence Reinflation

In our second suite of simulations, we model how the evolution of a hot Jupiter undergoing deposited heating is affected by the varying luminosity of the host star. To do so, we incorporate a time-dependent incident stellar flux $F_\star = L_\star/(4\pi a^2)$ using precalculated stellar evolution tracks from MIST models (Choi et al. 2016; Dotter 2016) to obtain the stellar luminosity $L_\star$. We assume a fixed planetary semimajor axis of $a = 0.04747$ au relevant for HD 209458b. We include deposited heating in the planet throughout the main-sequence evolution of its host star, keeping the fraction of

the incident stellar power converted to the deposited heating (γ) fixed with time. Note that though we keep γ fixed in our main grid of simulations, in Section 5.3 we include the inferred dependence of deposited heating on equilibrium temperature from Thorngren & Fortney (2018) in our evolution models. We stop these models when the host star reaches the end of the main sequence, which occurs at 9.88 Gyr for our simulations of planets orbiting a Sun-like star.

In both this suite of simulations and the suite studying post-main-sequence reinflation (described in Section 2.2.3), we keep the outer mass column in which irradiation is applied fixed at $\Sigma_p = 300$ g cm^{-2}. This corresponds to a visible opacity of $\kappa_{\rm vis} = 3.33 \times 10^{-3}$ cm^2 g^{-1} and a visible photosphere at 0.27 bars when the radius is equal to that of HD 209458b. We use this reduced visible opacity to aid with model stability at times in the host star evolution when the incident stellar flux rapidly increases. We show results from our main-sequence reinflation grid in Section 3.2.

2.2.3. Post-main-sequence Reinflation

Our third grid of simulations studies the evolution of warm Jupiters that reinflate while their host star evolves on the post-main sequence. In this suite of models, we only include deposited heating if the incident stellar flux $F_\star \geqslant 2.268 \times 10^8$ erg cm^{-2} s^{-1}, which corresponds to an equilibrium temperature $T_{\rm eq} \geqslant 1000$ K. We do so because gas giants with $T_{\rm eq} < 1000$ K do not have anomalous radii (Demory & Seager 2011; Laughlin et al. 2011; Miller & Fortney 2011; Lopez & Fortney 2016; Thorngren & Fortney 2018). Weak deposited heating in warm Jupiter interiors is also expected from the inferred dependence of deposited power on $T_{\rm eq}$ (Thorngren & Fortney 2018), which decreases to zero at $T_{\rm eq} < 1000$ K. This is also consistent with ohmic dissipation and models of atmospheric heat transport, which expect that planets with $T_{\rm eq} < 1000$ K should not be inflated, due to the small day–night forcing and low atmospheric ionization fraction (Youdin & Mitchell 2010; Menou 2012; Ginzburg & Sari 2016; Tremblin et al. 2017). As a result, we assume that there is no deposited heating for planets with $T_{\rm eq} < 1000$ K, because otherwise warm Jupiters with anomalously large radii would have been discovered. To support this assumption, we show in Section 5.1 that if gas giants with $T_{\rm eq} < 1000$ K did undergo deposited heating with a similar conversion rate of incident stellar power to deposited heat and heating depth as inflated hot Jupiters, warm Jupiters would likely be inflated as well.

In our post-main-sequence reinflation simulations, we study planets that lie at equilibrium temperatures below 1000 K for the majority of the time that their host stars are on the main sequence. As a result, the inflation mechanism heats the planet only after the host star is at or near the end of its main-sequence evolution. Our fiducial case is that of a warm Jupiter with an orbital separation of 0.1 au orbiting a Sun-like star, which corresponds to an equilibrium temperature of 882 K for the present-day solar luminosity. We use the same stellar evolution tracks as for our main-sequence reinflation models, but evolve our simulations until the host star reaches a radius of 10 $R_\odot$. This corresponds to an age of 11.27 Gyr for a planet orbiting a Sun-like star, which occurs while the star is on the red giant branch. We choose this stopping radius because it is challenging to detect Jupiter-sized planets around larger stars with current instrumentation (Lopez & Fortney 2016), and because after this point, the radius of the host star quickly grows and the planet would become engulfed. Results from these simulations studying post-main-sequence reinflation are shown in Section 3.3.

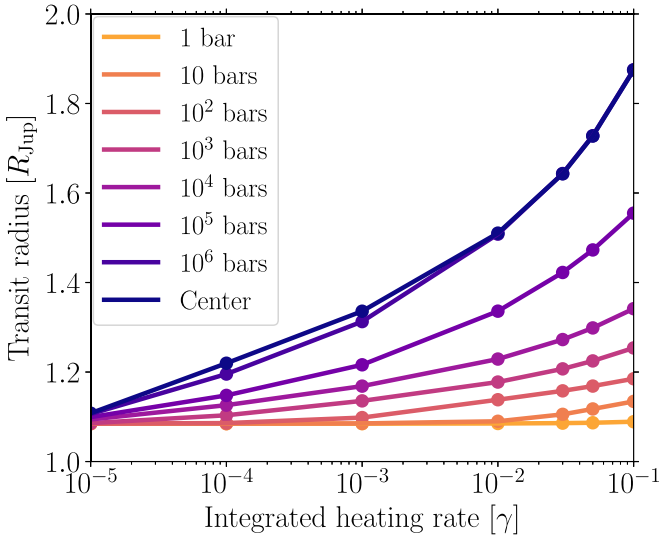

Figure 1. Planets that undergo deep heating can significantly reinflate. Shown is the transit radius in Jupiter radii after 10 Gyr of reheating for varying integrated heating rates ($\gamma = \Gamma/L_{\rm irr}$, from 10^{-5} to 0.1) and heating locations ($P_{\rm dep}$; from 1 bar to the planet center, with darker colors corresponding to deeper heating). Planets have the mass of HD 209458b and receive a fixed irradiation power of 2.4×10^{29} erg s^{-1}. We find that heating that is stronger and/or deeper leads to greater reinflation.

3. Results

3.1. Reinflation of an Evolved Hot Jupiter

To elucidate the process by which gas giants reinflate, we first analyze the results from our suite of idealized simulations of the reinflation of an evolved hot Jupiter. Figure 1 shows the transit radius after 10 Gyr of reheating for a hot Jupiter with an initial radius of 1.08 $R_{\rm Jup}$ for varying heating rates γ and heating depths $P_{\rm dep}$. Note that the pressure level of heating at the center of the planet depends on the heating rate, varying from 12.1 Mbar with a weak heating rate of $\gamma = 10^{-5}$ after 10 Gyr of reheating to 4.35 Mbar with a strong heating rate of $\gamma = 10^{-1}$ at the same age. To calculate the transit radius from the photospheric radius, we use the isothermal limit of Guillot (2010; see their Equation (60)) and set the ratio of visible to infrared opacities equal to 0.4, as in Komacek & Youdin (2017). We find that the transit radius increases monotonically with both integrated heating rate and heating depth. As a result, increasing either the heating rate or the heating depth leads to greater reinflation. We find that deep heating at or near the center of the planet can lead to significant reinflation, as in Lopez & Fortney (2016).

Comparing our results in Figure 1 for the effect of deposited heat on reinflation to the effect of deposited heat on slowing planetary cooling from Figure 3 of Komacek & Youdin (2017), we find significant differences. For reinflation, there is not a large increase in the transit radius between 10 and 100 bars, and the radius continues to increase with deeper heating within the interior (at pressures $P_{\rm dep} \geqslant 10^3$ bars), unlike that found in Komacek & Youdin (2017). This shows that, at a given age, the effects of deposited heating on reinflation are fundamentally different than the effects of heating on offsetting the cooling of

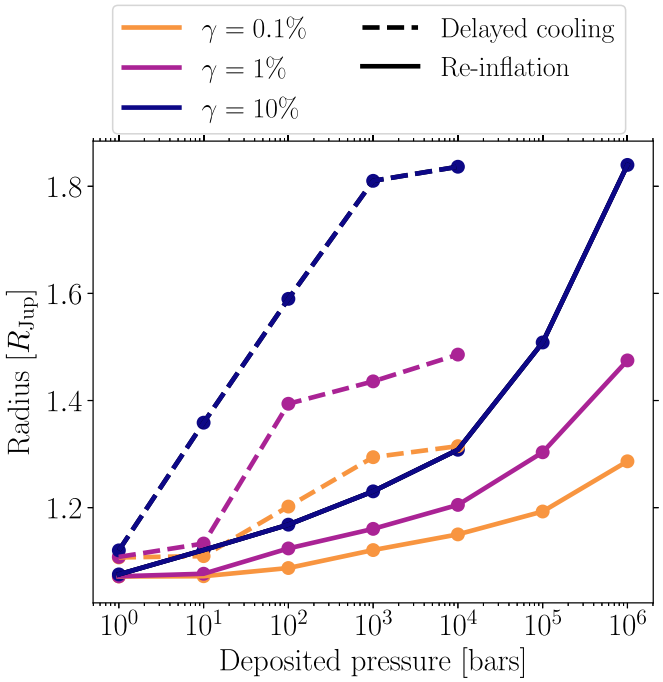

Figure 2. Heating needs to be deeper to reinflate planets than it does to delay planetary cooling. Shown is a comparison of our results for how reinflated planet radii after 5 Gyr of evolution depend on deposited pressure for varied integrated heating rates γ (solid lines) with the results of Komacek & Youdin (2017; dashed lines), who considered the effect of heating on delaying planetary cooling. We find that heating that leads to reinflation has to be at pressures of 10^6 bars or greater to reach a radius similar to that in delayed cooling models with heating deeper than 10^3 bars.

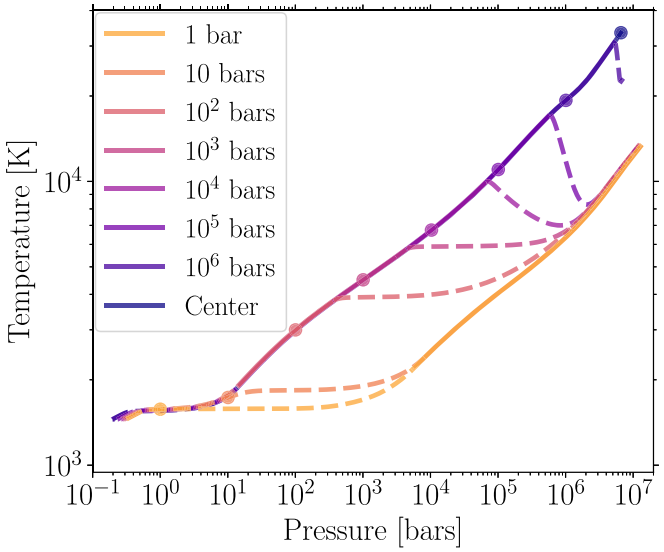

Figure 3. Deposited heating reinflates the interior of a planet from the outside in. Temperature–pressure profiles from simulations after 10 Gyr of reheating with an integrated heating rate of $\gamma = 1\%$ and varying deposition pressure from 1 bar to the planet center. Solid lines show convective regions, while dashed lines show nonconvective regions. Note that regions near the surface are radiative down to ≈10 bars. Circles show the maximal heating location, with the color of the circle the same as the matching temperature–pressure profile. The entire interior of the planet is convective only in the case with heating at the very center.

an initially high-entropy planet. However, we will show in Section 4 that the final equilibrium state (at a time $t = \infty$) of planets that undergo heating which leads to reinflation and that undergo heating which delays planetary cooling is the same.

Figure 2 directly compares our results for the effect of heating on reinflation and the results of Komacek & Youdin (2017) on the effect of heating on slowing planetary cooling. We find that reinflation requires heating at pressures $P_{\rm dep} \geqslant 10^6$ bars to reach the same radius at 5 Gyr as delayed cooling models with heating at pressures $P_{\rm dep} \geqslant 10^3$ bars. Unlike deposited heating that delays planetary cooling, the radii of reinflated planets after 5 Gyr continue to increase with deeper heating deposited below the inner radiative–convective boundary. Deposited heating that leads to reinflation heats the planet both upward and downward of the deposition level. Reinflation from the heating level upward (which we term "inside-out" reinflation) occurs very quickly, within $\lesssim$1 Myr in most cases. Meanwhile, the timescale to reheat the center (termed "outside-in" reinflation) can be as long as ~ Tyr and decreases with increasing depth of heat deposition (Ginzburg & Sari 2016). We explore the differences between inside-out and outside-in reinflation in detail in the Appendix.

Because the reinflation timescale scales inversely with the heating depth, deeper heating will lead to greater reinflation, unlike in the case of delayed cooling where deposited heating below the inner radiative–convective boundary (at $P_{\rm dep} > 10^3$ bars) leads to similar radii after 5 Gyr of evolution (Komacek & Youdin 2017). This is because heating that slows planetary cooling only has to balance cooling from the interior convective zone. Meanwhile, heating that reinflates an initially cold planet has to increase the entropy at the center of the planet rather than simply reduce the internal cooling rate. As long as it is deposited below the inner radiative–convective boundary, heating that acts to slow planetary cooling has almost the same effect on evolution regardless of deposition pressure, while the radius after the reheating of an initially cold planet continues to increase with deeper heating within the internal convective zone.

Figure 3 shows temperature–pressure profiles from simulations with a fixed heating rate of $\gamma = 1\%$ of the incident stellar power and varying heating depth. These temperature–pressure profiles are similar to those expected from the reinflation models of Wu & Lithwick (2013; see their Figure 7) and the theory of Ginzburg & Sari (2016; see their Figure 5). However, there are differences due to our use of localized heat deposition instead of the ohmic dissipation heating profiles considered in Wu & Lithwick (2013) and Ginzburg & Sari (2016), and generally different heating mechanisms will lead to significant differences in the temperature profile. We find that in the case of reinflation, heating forces regions at pressures less than $P_{\rm dep}$ to be convective, similar to the case of heating that slows planetary cooling (Komacek & Youdin 2017). However, as in Wu & Lithwick (2013), we find that heating that leads to reinflation forces a downward heat flux that acts to reinflate the planet from the heating level downward. As a result, the reinflation timescale is governed by the downward heat flux from the heating level. We stress that the cases shown in Figure 3 with $P_{\rm dep} \leqslant 10^5$ bars are still evolving, while the final equilibrium (discussed in Section 4) is characterized by an isotherm from the heating level to the center of the planet. We find that deposited heating that is not near the center has a relatively small effect on the central temperature and hence on the entropy of the internal adiabat after 10 Gyr of evolution. As a result, only heating near the center can lead to reinflation that greatly increases the radius of the planet over short timescales.

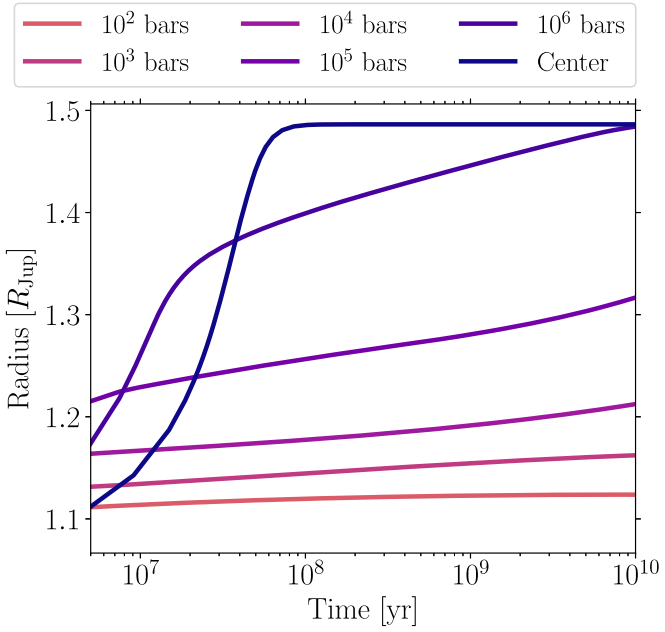

Figure 4. Reinflation takes billions of years if heating is not deposited at the very center of the planet. Radius evolution for simulations with a fixed heating rate of $\gamma = 1\%$, fixed incident stellar power of $L_{\rm irr} = 2.4 \times 10^{29}$ erg s^{-1}, and varying heating locations from 100 bars to the planet center. Only the simulation with heating at the very center reaches a steady state, while shallower heating models inflate over their evolution. The simulation with heating at $P = 10^6$ bars reaches a similar radius to the case with heating at the very center, while simulations with shallower heating reach smaller radii after reinflation. Figure 9 shows the radius evolution in an extension of these simulations to 10^{13} yr, by which point simulations with $\gamma = 1\%$ and $P_{\rm dep} > 10^2$ bars have reached a radius equilibrium.

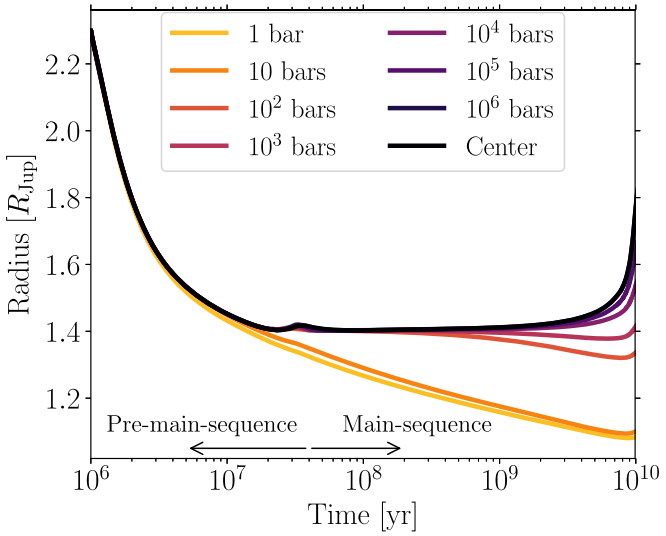

Figure 5. Radii of hot Jupiters that undergo deep heating evolve along with their host stars. Radius evolution for simulated hot Jupiters orbiting a star with the stellar evolution track of the Sun and a fixed heating rate of $\gamma = 1\%$ for varying heating locations from 1 bar to the planet center. The distinction between the pre-main-sequence and main-sequence phase of stellar evolution is shown by the arrows. Simulated planets have the mass and semimajor axis of HD 209458b. Heating must be deeper than 100 bars to lead to reinflation over the stellar main sequence, and deeper heating leads to larger inflation over the stellar main-sequence lifetime.

We find from our simulations that the timescale to reinflate a planet decreases with increasing heating depth. Figure 4 shows the radius evolution of simulations with fixed $\gamma = 1\%$ of the incident stellar power and varying heating depth. We find that the reinflation timescale for heating at the center of the planet is $\lesssim$50 Myr, comparable to the initial cooling timescale before heating acts to slow planetary cooling (before regime 2 of Komacek & Youdin 2017). Deep heating at 10^6 bars that is near the center can reinflate planets to the same radius as central heating, but it requires billions of years over which the planet can reinflate. Meanwhile, shallow heating at pressures $<10^3$ bars does not greatly affect the radius even after 10 Gyr of evolution. We will show in Section 4 that the long evolutionary timescales for planets with shallow heating are the cause of the differences in the dependence of radius on heating depth for reinflation relative to delayed cooling shown in Figure 2. To summarize, we expect that shallow heating at pressures $\lesssim 10^2$ bars will not lead to reinflation, moderately deep heating at pressures $10^3 \lesssim P_{\rm dep} \lesssim 10^5$ bars will lead to moderate reinflation, and deep heating at pressures $\gtrsim 10^6$ bars will greatly reinflate planets.

3.2. Main-sequence Reinflation

Now we analyze the results from our suite of models studying the main-sequence reinflation of hot Jupiters. Figure 5 shows radius evolution tracks for simulations with $\gamma = 1\%$ of the evolving incident stellar power and varying heating depth. We find that depending on the heating depth, the radius evolution of hot Jupiters while their stars are on the main sequence can be classified into three regimes. With shallow heating that does not extend below pressures of $\sim$10 bars, heating does not greatly affect the radius and the planet perpetually cools—this is analogous to regime 2(d) of Komacek & Youdin (2017). With moderately deep heating at 10^2 bars $\lesssim P_{\rm dep} \lesssim 10^3$ bars, heating delays planetary cooling (as in regime 2(c) of Komacek & Youdin 2017) but does not cause main-sequence reinflation. In the case of deep heating at pressures $\gtrsim 10^4$ bars (analogous to regimes 2(a) and 2(b) of Komacek & Youdin 2017), main-sequence reinflation can occur. Note that the boundary between the moderately deep heating regime with 10^2 bars $\lesssim P_{\rm dep} \lesssim 10^3$ bars and the deep heating regime with $P_{\rm dep} \gtrsim 10^4$ bars depends on the host stellar type—in principle, cases with $P_{\rm dep} \gtrsim 10^2$ bars will reinflate if stellar main-sequence evolution timescales are long enough. In the case of heating at the very center of the planet, main-sequence reinflation can be significant, with a $\sim$30% increase in the planetary radius over the main-sequence lifetime of the host star for $\gamma = 1\%$.

The main-sequence radius increase from our full suite of simulations with varying integrated heating rate and heating depth is shown in Figure 6. We quantify the main-sequence radius increase as the increase in planetary radius between the end of the pre-main sequence at 39.75 Myr and the end of the main-sequence stellar evolution at 9.88 Gyr. We find that heating at the center of the planet leads to main-sequence reinflation if the integrated heating rate $\gamma \gtrsim 0.1\%$. We also find that shallower heating at pressures $P_{\rm dep} \geqslant 10^3$ bars can lead to main-sequence reinflation, given sufficiently strong heating rates of $\gamma \geqslant 1\%$. The heating rates needed to explain main-sequence reinflation from our model suite are consistent with the $0.1\% \lesssim \gamma \lesssim 3\%$ heating efficiency needed to explain the sample of hot Jupiters with central heat deposition found by Thorngren & Fortney (2018). We will directly incorporate the prescription of Thorngren & Fortney (2018) to show that main-

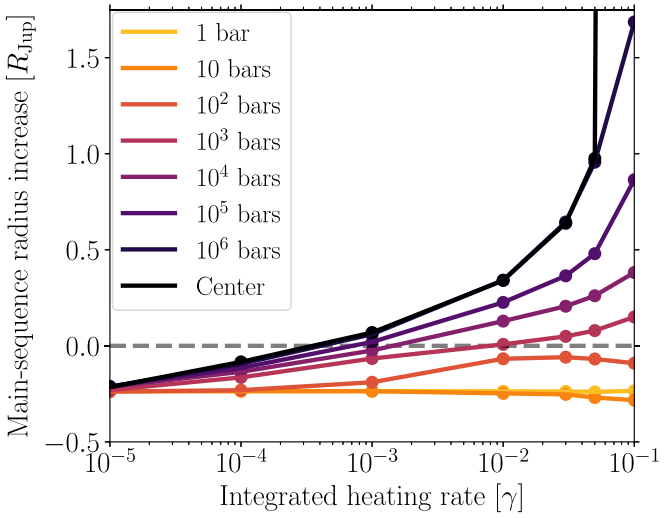

Figure 6. Reinflation of hot Jupiters during stellar main-sequence evolution can only occur with heating deeper than 1 kbar. Shown is the change in planetary radius over the main-sequence stellar evolution phase of the host star from simulations with varying heating rate and deposition pressure. The horizontal dashed line denotes a radius change of zero. Planets below this line shrink over their host stars' main-sequence evolution, while planets above this line reinflate over main-sequence evolution. We find that heating must be applied at pressures $\gtrsim 10^3$ bars to reinflate planets over the solar main sequence. If heating occurs at the very center of the planet, the heating rate must be $\gtrsim$0.1% of the incident stellar power to cause main-sequence reinflation.

sequence reinflation can be explained using their derived heating rates in Section 5.3.

3.3. Post-main-sequence Reinflation

Lastly, we show results from our suite of models studying the reinflation of warm Jupiters while their host stars are on the post-main sequence. Figure 7 shows radius evolution tracks for simulations with an integrated heating rate of $\gamma = 1\%$ of the evolving incident stellar power and varying heat deposition pressure. The planet cools over the first 8 Gyr of evolution, after which the equilibrium temperature of the planet is $\geqslant$1000 K (see inset in the left-hand panel of Figure 7) and the heating mechanism turns on. We find that deep heating at $P_{\rm dep} \geqslant 10^6$ bars leads to rapid reinflation during the late main sequence (after $T_{\rm eq}$ reaches 1000 K) with a large increase in the radius during the post-main-sequence evolution of the host star. For moderate heating depths 10^2 bars $\lesssim P_{\rm dep} \lesssim 10^5$ bars, there is only modest reinflation during the late main-sequence phase where $T_{\rm eq} \geqslant 1000$ K but a rapid increase in the planetary radius occurs as the star brightens and approaches the stopping point of $10\,R_\odot$. For shallow heating at pressures $\leqslant$10 bars, post-main-sequence reinflation does not occur (not shown). Overall, we find that the radius of the planet is tightly linked to the evolving incident stellar flux from the host star, as we found in Section 3.2 for the case of main-sequence reinflation.

Figure 8 shows the transit radius when the host star reaches $10\,R_\odot$ from our full suite of simulations of warm Jupiters with varying integrated heating rate and depth. We find that deep heating can greatly reinflate planets, even with relatively weak heating rates of $\gamma \lesssim 0.1\%$. With stronger heating, deep heating at $P_{\rm dep} \gtrsim 10^5$ bars can lead to a runaway in planetary radius, leading to Roche lobe overflow (Valsecchi et al. 2015; Jackson et al. 2017), as found by Batygin et al. (2011). This is also why the cases with heating at pressures $\geqslant 10^5$ bars shown in Figure 7 inflate to larger than $2\,R_{\rm Jup}$. These large radii are caused by the positive feedback between planetary radius, incident stellar power, and deposited heating rate. Larger planets receive more incident stellar power for a given incident stellar flux, which leads to larger deposited heating rates assuming a fixed conversion of incident stellar power to deposited heat. These larger heating rates lead to an increase in the planetary radius, which feeds back and increases the heating rate further, causing a runaway in the planetary radius. Note that we show in Section 5.3 that this runaway likely would not occur if the deposited heating peaks at an intermediate value of incident flux, as expected for the sample of hot Jupiters (Thorngren & Fortney 2018).

Figure 8 also shows that relatively shallow heating at pressures 10^2 bars $\lesssim P_{\rm dep} \lesssim 10^4$ bars with high heating rates $\gamma \gtrsim 1\%$ can lead to the same radius as deep heating at $P_{\rm dep} \gtrsim 10^5$ bars with weak heating rates $\gamma \lesssim 0.1\%$. At face value, this implies that the degeneracy between the heating rate and heating depth still applies in the case of post-main-sequence reinflation. However, we will discuss in Section 5.2 how this degeneracy can be broken by also considering the evolutionary stage of the host star.

4. Reinflation by Point-source Energy Deposition

To interpret our results, we consider the analytic theory of Ginzburg & Sari (2015, 2016) for the structure of a planet heated by energy that is deposited at a point within the planetary interior. In this theory, we assume that a heating luminosity Γ is deposited at an optical depth $\tau_{\rm dep}$. This is a simplification of the actual heating profiles in our numerical simulations, but as we will show accurately reproduces the key features of our numerical results. Additionally, we parameterize the convective profile as in Ginzburg & Sari (2015):

$$\frac{U}{U_c} = \left(\frac{\tau}{\tau_c}\right)^{\beta}, \tag{10}$$

where $U = a_{\rm rad}T^4$ is the radiative energy density with $a_{\rm rad}$ the radiation constant. U_c and τ_c are the radiation energy density and optical depth at the center of the planet, respectively, and β is related to the opacity profile and planetary structure as shown in Equation (3) of Ginzburg & Sari (2015).

We further consider the final end state at $t = \infty$, which we term the "equilibrium" stage of planetary evolution, at which point the planetary structure is in a steady state. This equilibrium state is Stage 4 in the evolution under deposited heating described in Appendix A of Ginzburg & Sari (2016). Figure 7 of Ginzburg & Sari (2016) shows the expected temperature profile at equilibrium. This temperature profile is radiative and nearly isothermal from the outside to the outer radiative–convective boundary located at $\tau_{\rm rcb} = 1/\gamma$ (Equation (11) of Ginzburg & Sari 2015), follows the convective power-law profile in Equation (10) from $\tau_{\rm rcb}$ to the heating location $\tau_{\rm dep}$, and is isothermal from below the heating level to the center of the planet. At equilibrium, the central temperature T_c is set by the heating rate γ and depth $\tau_{\rm dep}$ and is given by Equation (25) of Ginzburg & Sari (2015):

$$\frac{T_c}{T_{\rm eq}} \sim (1 + \gamma\tau_{\rm dep})^{\beta/4}. \tag{11}$$

For inflation that is small compared to the initial size of the planet, the increase in radius ΔR is directly proportional to the central temperature (see Equation (29) of Ginzburg &

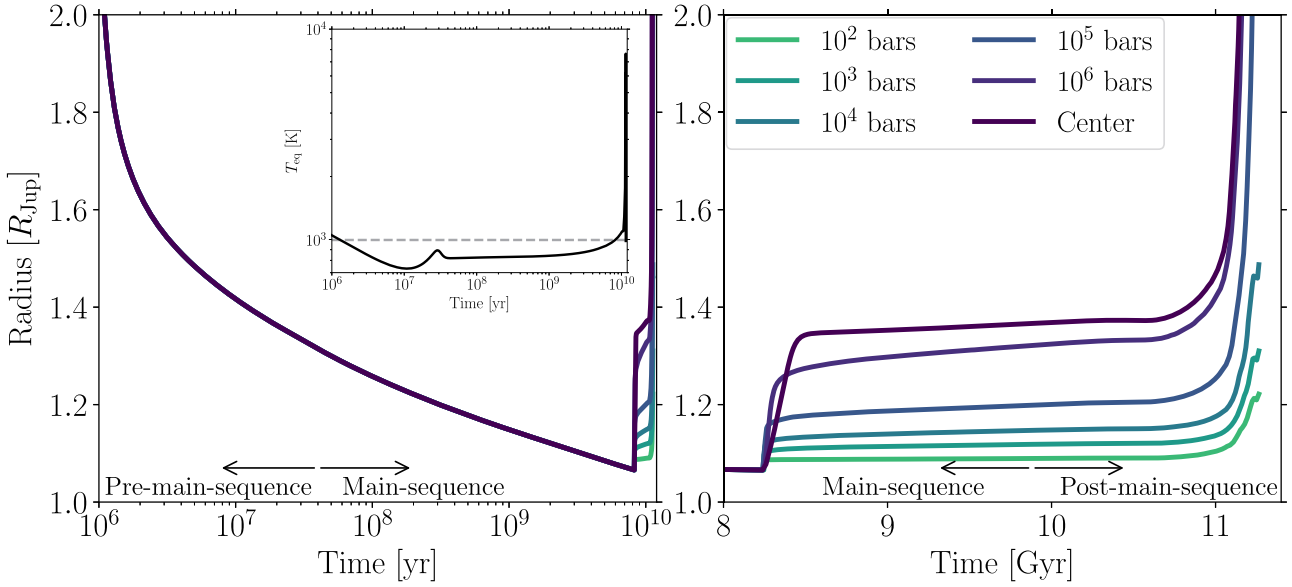

Figure 7. Post-main-sequence stellar evolution leads to abrupt inflation of warm Jupiters. The left-hand panel shows the radius evolution of a warm Jupiter orbiting at 0.1 au from its host star for varying deposition pressures from 100 bars to the center and a fixed heating rate of $\gamma = 1\%$. The inset shows the corresponding equilibrium temperature evolution using MIST solar evolution tracks (Choi et al. 2016; Dotter 2016), and the dashed line in the inset shows the $T_{\rm eq} = 1000$ K threshold above which deposited heating occurs. The right-hand panel shows late evolutionary stages in which planets become reinflated. The distinction between pre-main-sequence and main-sequence evolutionary stages is shown by the arrows in the left-hand panel, and the main-sequence and post-main-sequence phases are marked by arrows in the right-hand panel. In this set of models, we assume that heating only occurs when $T_{\rm eq} \geqslant 1000$ K, as warm Jupiters are observed to not have inflated radii (Miller & Fortney 2011; Thorngren & Fortney 2018). There are two increases in radius after 8 Gyr: the first is due to the equilibrium temperature reaching 1000 K, at which point the heating mechanism turns on, and the second occurs as the star brightens on the post-main sequence. We confirm the results of Lopez & Fortney (2016) that deep heating can significantly reinflate warm Jupiters. We also find that relatively shallow heating at pressures $\gtrsim$100 bars can lead to significant reinflation.

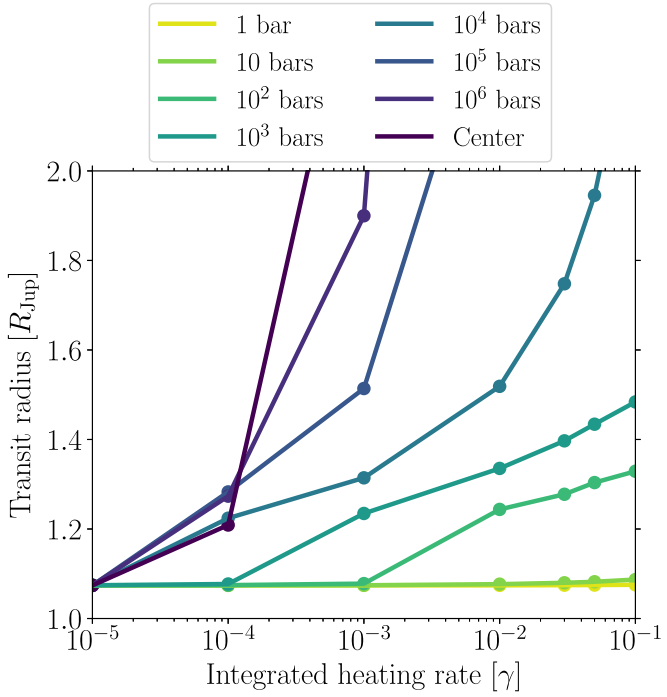

Figure 8. Warm Jupiters that undergo deep heating will greatly reinflate during post-main-sequence stellar evolution. Shown are the transit radii in units of Jupiter radius for warm Jupiters with the mass of HD 209458b orbiting a Sun-like star at a semimajor axis of 0.1 au. The transit radii are shown at the time when the host star has evolved to a radius of 10 $R_\odot$. The transit radii are shown for varying integrated heating rates ($\gamma = \Gamma/L_{\rm irr}$; from 10^{-3}% to 10%) and heating locations ($P_{\rm dep}$; from 1 bar to the planet center). We find that heating at pressures $\geqslant$100 bars is required for reinflation, while deep heating at pressures $\gtrsim 10^4$ bars can lead to a more than doubled radius during post-main-sequence stellar evolution.

Sari 2015). As a result, using Equation (11), we can derive a scaling for the dependence of the increase in radius on heating rate γ and heating depth $\tau_{\rm dep}$:

$$\Delta R \propto (\gamma \tau_{\rm dep})^{\beta/4}. \quad (12)$$

To compare the analytic theory described above to our numerical results, we extend our idealized simulations of reinflation from Section 3.1 out to 10 Tyr, at which point the simulations with heating at $P_{\rm dep} \geqslant 10^3$ bars reach a final equilibrium. Figure 9 shows the radius evolution and final temperature–pressure profiles of a subset of these simulations with $\gamma = 1\%$ and $P_{\rm dep} \geqslant 10^3$ bars. We find that all simulations shown reach radius equilibrium by 10 Tyr. Cases with $\gamma = 1\%$ and $P_{\rm dep} \leqslant 10^2$ bars cool below the limits of the MESA equation of state,[6] as their central temperatures drop below ~5000 K after ~ Tyr of evolution. As a result, simulations with shallow heating do not reach equilibrium, and we do not compare them to our analytic theory.

The temperature–pressure profiles in Figure 9 are characterized by a nearly isothermal outer radiative zone, a convective zone which extends from the radiative–convective boundary to the bottom of the heating level, and an inner radiative zone that is isothermal from the bottom of the heating level to the center of the planet. Planets reach this final structure through reheating both from the heating level outward toward the surface and from the heating level downward toward the center. Figure A1 in the Appendix shows that the "inside-out" heating that leads to the formation of a convective region from the outer radiative–convective boundary to the heating level occurs quickly (within 1 Myr). Inside-out reinflation is unique to the

[6] This is the region labeled "here be dragons" in Figure 50 of Paxton et al. (2019).

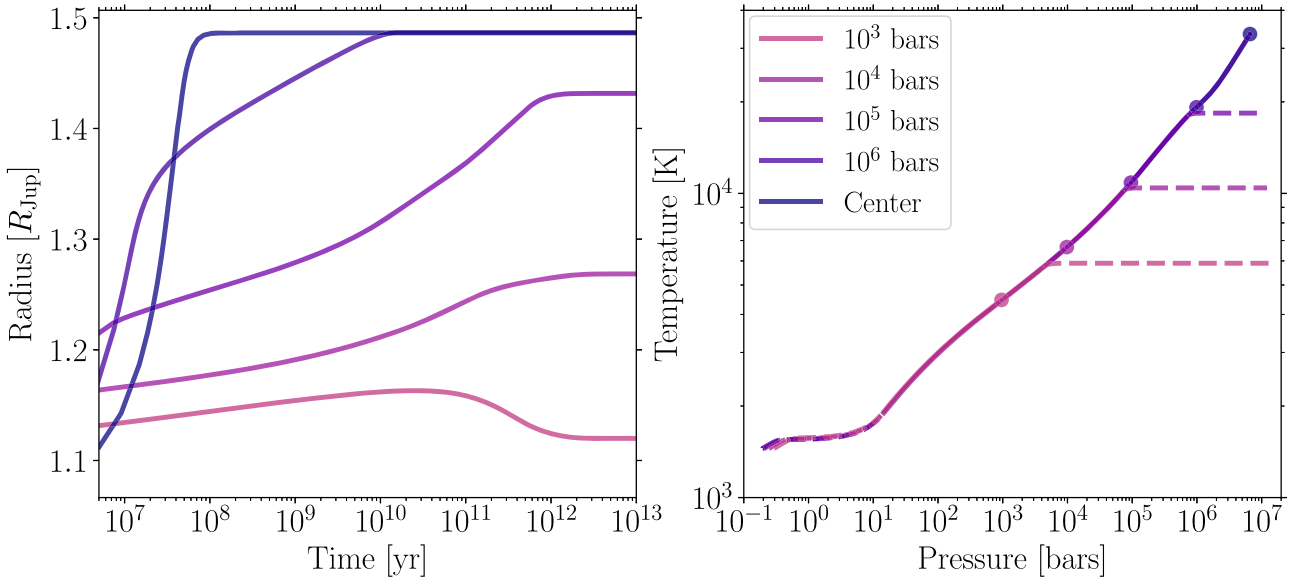

Figure 9. Reinflation can take tens to thousands of Gyr if heating is not at the center of the planet, where the final equilibrium includes a deep isotherm from the bottom of the heating level to the center of the planet. Left-hand panel: the radius evolution from simulations with $\gamma = 1\%$ and varying $P_{\rm dep}$ from 10^3 bars to the planet center. This panel shows the continued evolution of simulations from Figure 4 out to 10 Tyr. Simulations with heating at $P_{\rm dep} \leqslant 10^5$ bars take $\sim$1 Tyr or longer to reach an equilibrium state. Right-hand panel: the temperature–pressure profiles from the end state of the same simulations as shown in the radius evolution tracks. Solid lines show adiabatic regions, while dashed lines correspond to nonconvective regions. Points show the maximal heating locations for each $P_{\rm dep}$. The deep structure of each case is characterized by an isotherm leading from the bottom of the heating level to the center of the planet. This equilibrium state from reinflation is the same as in the case of a planet that undergoes delayed cooling due to deposited heating (Ginzburg & Sari 2015, 2016).

case of point-source heat deposition, as reinflation due to heating that decays from the surface inward as considered in Wu & Lithwick (2013) and Ginzburg & Sari (2016) only leads to outside-in reinflation. The equilibrium structure from our numerical simulations is the same structure as was predicted by Ginzburg & Sari (2016) to occur at the equilibrium stage of planetary evolution. As a result, the final state of hot Jupiters that undergo reinflation is the same as the final state of hot Jupiters that undergo delayed cooling, due to deposited heating.

We compare our theoretical scaling for the dependence of the equilibrium radius on $\gamma\tau_{\rm dep}$ from Equation (12) to that at the final state of our numerical simulations with varying γ and $P_{\rm dep}$ in Figure 10. We calculate β from our numerical simulations, finding that $\beta = 0.348$, in agreement with the value of 0.35 expected from Ginzburg & Sari (2015). As discussed above, we do not include simulations with $P_{\rm dep} \leqslant 10^2$ bars in this comparison because they do not reach a final equilibrium state in the simulated time frame. We find that the analytic scaling broadly matches the numerical results for the dependence of radius on the product $\gamma\tau_{\rm dep}$. This differs from the results of Komacek & Youdin (2017) (see their Figure 10), where the dependence of radius on $\gamma\tau_{\rm dep}$ was not uniform with $P_{\rm dep}$. This is because our reinflation models are evolved to a true equilibrium state, while the comparison with the delayed cooling models of Komacek & Youdin (2017) was done after 5 Gyr of evolution, before the final equilibrium state is reached. As a result, the theory of Ginzburg & Sari (2015, 2016) can be used to determine the planetary structure for the final equilibrium state at $t = \infty$ given the combination of heating rate and depth, as in the equilibrium state the heating rate and depth together set the central temperature and radius of the planet. After 10 Gyr of evolution, only some models with deep heating at $P_{\rm dep} \gtrsim 10^6$ bars reach this equilibrium, while others with shallower heating are still evolving. The long timescales to reach equilibrium for shallow heating that leads to reinflation

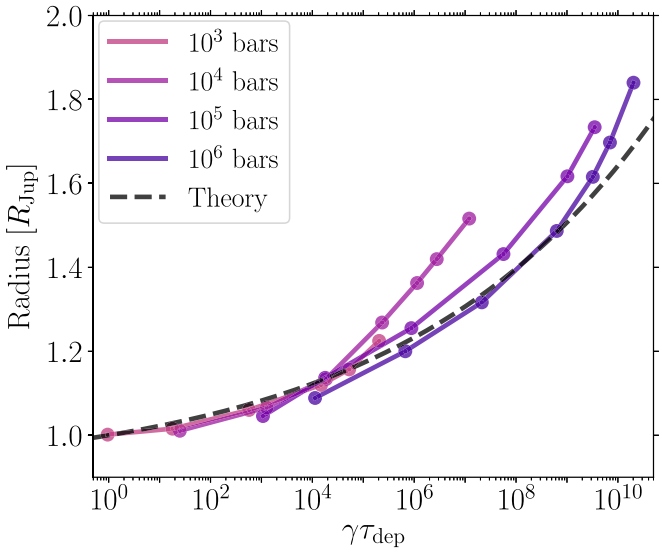

Figure 10. Analytic theory of Ginzburg & Sari (2015) captures the dependence of equilibrium radius on heating rate and depth found in our suite of idealized models of reinflation. Solid lines that connect points show the equilibrium radius from our numerical simulations as a function of the product of the normalized heating rate γ and optical depth of the maximal heating location $\tau_{\rm dep}$. The dashed line shows our analytic prediction for the dependence of radius on $\gamma\tau_{\rm dep}$ from Equation (12). We find that the analytic prediction agrees with the general trend of increasing radius with increasing $\gamma\tau_{\rm dep}$ found in the end state of our numerical simulations.

are the cause of the differences we found in Section 3.1 between heating that delays planetary cooling and heating that leads to reinflation.

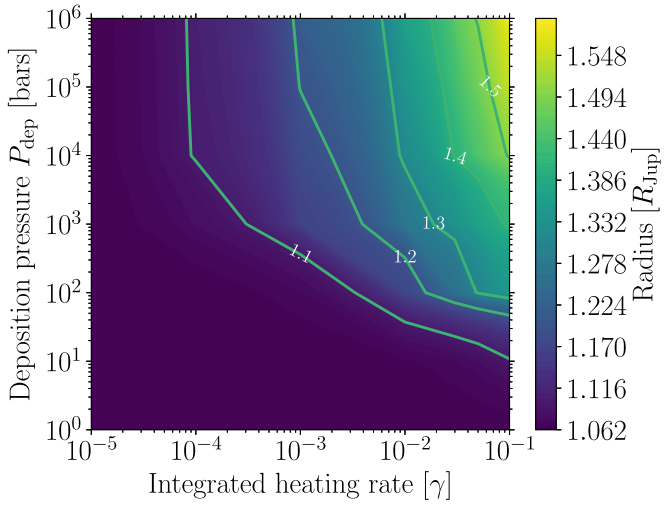

Figure 11. Warm Jupiters would be significantly inflated if they underwent deep heating during the main-sequence evolution of their host stars. Contours show the radius at the end of stellar main-sequence evolution for varying heating rate and deposition pressure for a warm Jupiter with the mass of HD 209458b orbiting a Sun-like star at a semimajor axis of 0.1 au. In this set of simulations, we do *not* assume that heating only occurs when $T_{\rm eq} \geqslant 1000$ K, and allow heating to continue below this limit. We find that warm Jupiters are inflated if a heating rate of $\gtrsim$1% of the incident stellar power is deposited deeper than $\sim 10^3$ bars. The fact that no inflated warm Jupiters have been found (Demory & Seager 2011; Miller & Fortney 2011; Thorngren & Fortney 2018) means that if warm Jupiters undergo deposited heating, it is too weak and/or too shallow to lead to inflation.

5. Discussion

5.1. Main-sequence Reinflation

A key result from this work is that hot Jupiters evolve along with their host stars. For sufficiently deep and strong heating, we expect the radii of hot Jupiters to increase as their host stars brighten. For heating at the very center of the planet, radii can increase by a factor of 2 over stellar main-sequence evolution. Due to the long timescales of reinflation, we find that the greatest amount of main-sequence reinflation occurs between 1 and 10 Gyr of evolution. As a result, precise stellar ages (using precise stellar parameters derived from asteroseismology and spectral characterization; e.g., Grunblatt et al. 2016, 2017, 2019) are critical for understanding the mechanism that inflates hot Jupiters.

The observation of a lack of inflated warm Jupiters (Demory & Seager 2011; Laughlin et al. 2011; Miller & Fortney 2011; Thorngren & Fortney 2018; Thorngren et al. 2019) points toward weak heating rates and/or shallow heat deposition for planets with $T_{\rm eq} < 1000$ K. Note that it also might point toward a weaker atmospheric circulation because the planet is not tidally locked, as found by previous studies of the atmospheric circulation of warm Jupiters (Showman et al. 2015; Rauscher 2017; Ohno & Zhang 2019). To determine the threshold of the combination of heating rate and deposition pressure that would cause warm Jupiters to be inflated, we explored the effects of heating on main-sequence evolution of warm Jupiters. To do so, we used the same setup as our main-sequence evolution model suite but studied the evolution of a warm Jupiter at a semimajor axis of 0.1 au. Our results for the radius of these warm Jupiters after the main-sequence evolution of a Sun-like star are shown in Figure 11. We find that warm Jupiters would be inflated for integrated heating rates of $\gamma \gtrsim 0.1\%$ and heating depths $P_{\rm dep} \gtrsim 10^3$ bars.

Because no inflated warm Jupiters have been observed, we infer that the same heating mechanism that inflates hot Jupiters likely does not act to inflate warm Jupiters orbiting main-sequence stars. This finding confirms the validity of our assumption that reinflated warm Jupiters orbiting post-main-sequence stars are not inflated while their host stars were on the main sequence. The weak deposited heating in warm Jupiters agrees with the inferred decrease in deposited heating rate for hot Jupiters at low incident stellar flux (Thorngren & Fortney 2018). This is additional evidence that the radii of close-in gas-giant planets are directly tied to the evolution of their host stars through changes in the incident stellar flux. Additionally, the lack of inflation of warm Jupiters orbiting main-sequence host stars simplifies the interpretation of reinflated warm Jupiters orbiting post-main-sequence stars, because it is not necessary to determine how inflated the planet was before $T_{\rm eq} > 1000$ K.

5.2. Post-main-sequence Reinflation

The three candidate reinflated warm Jupiters orbiting post-main-sequence stars characterized by Grunblatt et al. (2016, 2017, 2019) all have similar radii of $\approx$1.3–1.45 $R_{\rm Jup}$ and orbit stars slightly more massive than the Sun. We can explain the radii of these planets in the context of our simulations with either strong heating ($\gamma \sim 1\%$ of the incident stellar flux) that is deposited shallow (at $P_{\rm dep} \lesssim 10^4$ bars) or with weak heating ($\gamma \sim 0.01$–0.1%) that is deposited deep (at $P_{\rm dep} \geqslant 10^5$ bars). Our results for the deep heating scenario are consistent with the heating rates required by Grunblatt et al. (2017) to explain the transit radii of K2-97b and K2-132b.

Though we find a degeneracy between the inferred heating rate and depth needed to explain reinflated warm Jupiters, we propose that there are two ways that this degeneracy can be broken. The first is that if heating is deep, we predict that the radii of warm Jupiters will sharply increase as their host star continues to evolve on the post-main sequence. As a result, if reinflated warm Jupiters with radii approaching or exceeding $2R_{\rm Jup}$ are detected orbiting evolved post-main-sequence stars, then the heating that causes reinflation must be deep. The second way to break the degeneracy between heating strength and heating depth is to study the time evolution of radii of reinflated warm Jupiters by obtaining precise stellar ages for evolved host stars of reinflated warm Jupiters. We expect that deep heating is needed to cause rapid reinflation when the heating mechanism turns on at $T_{\rm eq} \geqslant 1000$ K. If reinflated warm Jupiters are found during this late main-sequence phase, then the heating mechanism must be deep. Conversely, if warm Jupiters are not found to be inflated during this late main-sequence phase but are inflated on the post-main sequence, then the heating must be concentrated at $P_{\rm dep} \lesssim 10^5$ bars.

The stellar post-main-sequence evolution timescale decreases for more massive stars. As a result, we expect that heating at different depths will result in different stellar mass distributions for reinflated warm Jupiters, as less massive stars have longer evolutionary timescales that allow for greater reinflation. Additionally, there will be a threshold mass above which post-main-sequence reinflation of warm Jupiters cannot occur due to the short stellar evolution timescales. For central heating, which has the shortest reinflation timescale of all of our heating depths considered, the heating timescale is $\sim$50 Myr with $\gamma = 1\%$. Complete reinflation can only occur for warm Jupiters orbiting stars with post-main-sequence

lifetimes comparable to or longer than the heating timescale. Note that the heating timescale itself will also depend on stellar class, because with a fixed conversion of incident stellar power to deposited heating planets orbiting earlier-type stars will undergo a larger total heating rate. Additionally, the stellar evolution timescale must be short enough for the host star to reach the post-main sequence by the present day. Including both these constraints, we expect that reinflated warm Jupiters will be most prevalent around stars with masses $1M_{\odot} \lesssim M_{\star} \lesssim 1.5M_{\odot}$. This is the mass range in which current detections of reinflated warm Jupiters orbiting post-main-sequence stars have been made (Grunblatt et al. 2016, 2017, 2019).

5.3. Using Reinflation to Test Radius Inflation Mechanisms

To determine if the inferred heating derived by Thorngren & Fortney (2018) from the full sample of hot Jupiters can lead to reinflation, we ran two additional simulations. One simulation used the same setup as our main-sequence reinflation suite, while the other used the same setup as our post-main-sequence evolution suite—the only difference was that in both simulations, we used central heating, with the integrated heating rate dependent on the incident stellar flux as in Equation (34) of Thorngren & Fortney (2018). In this model, the heating rate is a Gaussian with a peak at an intermediate value of the incident stellar flux that corresponds to an equilibrium temperature of $\approx$1600 K. Figure 12 shows the evolution of radius and integrated heating rate from these two simulations. We find that in both simulations, the heating rate increases and then decreases as the star brightens. However, the radius remains significantly inflated for both cases, even though it slightly decreases at late times in the post-main-sequence evolution case as the heating rate becomes weak. As a result, we find that the inferred heating rate for the sample of hot Jupiters can explain both main-sequence reinflation of hot Jupiters and post-main-sequence reinflation of warm Jupiters. This implies that deep heating mechanisms that weaken in integrated heating rate relative to the incident stellar power at high incident stellar flux may be viable to explain both main-sequence and post-main-sequence reinflation. Thorngren et al. (2019) recently showed that the strong heating rates required to explain the radii of hot Jupiters imply that the radiative–convective boundaries of hot Jupiters lie at pressures of 1–100 bars, shallower than the $\sim$1 kbar pressures expected from models without additional heating. Such shallow radiative–convective boundaries are consistent with our findings of main-sequence reinflation, as we expect that inflated planets will have outer radiative–convective boundaries at $\sim$10 bars. Additionally, this shallow radiative–convective boundary is consistent with the expectation from simulations of atmospheric dynamics of hot Jupiters that the deep atmosphere should be nearly adiabatic (Tremblin et al. 2017; Sainsbury-Martinez et al. 2019).

In this work, we found that shallow heating at $P_{\rm dep} \gtrsim 1$ kbar is sufficient to explain main-sequence reinflation, but that deep heating near the center of the planet is required to explain rapid reinflation of warm Jupiters. If the heating mechanism leads to deep heating, it can lead to both main-sequence and post-main-sequence reinflation. However, if the heat is deposited at shallow levels, it will not lead to significant reinflation of warm Jupiters while the host star is on the main sequence, even when $T_{\rm eq} > 1000$ K. Additionally, shallow heating will not lead to rapid post-main-sequence reinflation and can only lead to inflation up to $\sim$1.5 $R_{\rm Jup}$ (see Figure 8). It is possible that main-sequence and post-main-sequence reinflation are caused by different heating mechanisms. In this case, the mechanism that causes post-main-sequence reinflation would lead to deep heat deposition, while the (separate) mechanism that causes main-sequence reinflation would lead to relatively shallow heat deposition.

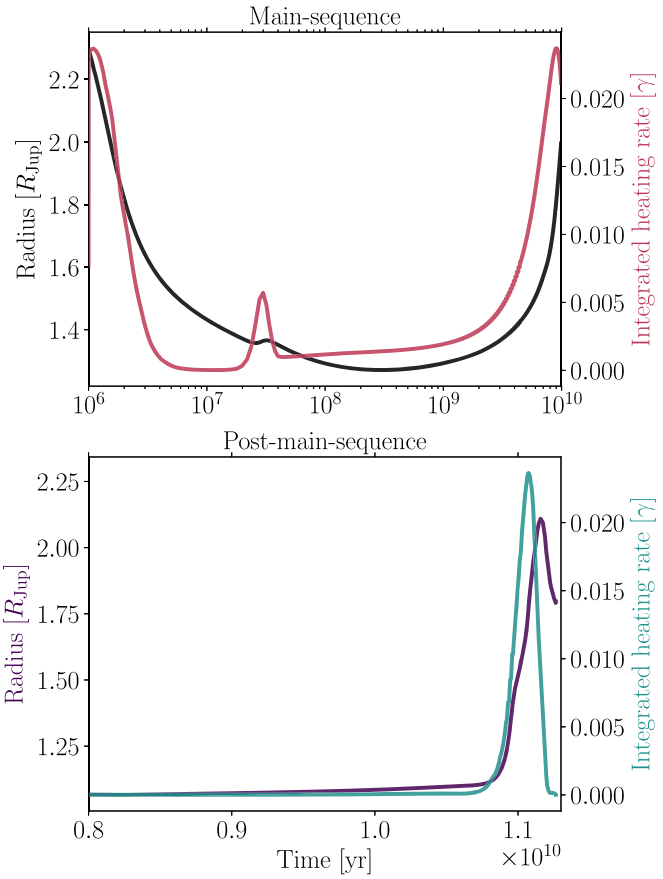

Figure 12. Heating required to explain the radii of the full sample of hot Jupiters can lead to both main-sequence and post-main-sequence reinflation. Shown is the radius evolution for the integrated heating rate inferred by Thorngren & Fortney (2018) from the sample of observed hot Jupiters. The radius evolution is shown on the left-hand y-axis, while the heating rate is shown on the right-hand y-axis. The top panel shows the main-sequence evolution of hot Jupiters, with a numerical setup similar to our simulations in Section 3.2. The bottom panel shows the post-main-sequence evolution of warm Jupiters, with a setup similar to that in Section 3.3. Note that time is on a logarithmic scale in the top panel and on a linear scale on the bottom panel, which focuses on post-main-sequence evolution. The heating rate is taken from Equation (34) of Thorngren & Fortney (2018) and is Gaussian with a peak at an equilibrium temperature of $\sim$1600 K. We find that the dependence of the inferred heating power on incident flux for the full hot Jupiter sample is consistent with both main-sequence reinflation of hot Jupiters and post-main-sequence reinflation of warm Jupiters.

We can relate the possibility of different heating depths for main-sequence and post-main-sequence reinflation discussed above to distinct proposed heating mechanisms. For instance, the post-main-sequence reinflation of warm Jupiters could be due to a nonzero initial eccentricity that enables strong tidal dissipation as the host star evolves off the main sequence, while the main-sequence reinflation of hot Jupiters could be caused by mechanisms related to atmospheric circulation (e.g., ohmic dissipation or an atmospheric heat flux directed inward). This is consistent with the expectation from previous work (Wu & Lithwick 2013; Ginzburg & Sari 2016; Lopez & Fortney 2016)

that ohmic dissipation will not lead to rapid reinflation. Additionally, both shallow and deep heating mechanisms could act together to cause reinflation. Notably, if tidal dissipation provides a deep heat source for warm Jupiters orbiting post-main-sequence stars, we would expect it to occur for only the fraction of planets that still have a nonzero eccentricity as the host star evolves off the main sequence. This is because tidal damping timescales for warm Jupiters orbiting Sun-like stars are on the order of Gyr (Gu et al. 2003; Grunblatt et al. 2017). As a result, we expect that tidal dissipation will not be a ubiquitous process for warm Jupiters orbiting post-main-sequence stars.

Future observations of a wide sample of reinflated warm Jupiters will test mechanisms for radius inflation. TESS will observe ∼400,000 evolved stars, with an expected $0.51\% \pm 0.29\%$ occurrence rate of close-in reinflated warm Jupiters around post-main-sequence stars (Grunblatt et al. 2019). As a result, we expect that TESS will discover a large sample of reinflated warm Jupiters. This large sample will directly test how deep deposited heating needs to be to reinflate warm Jupiters. If heating occurs near the center of the planet, warm Jupiters will undergo fast reinflation and TESS will find highly inflated planets with radii approaching the Roche limit. If heating is instead relatively shallow, there will be a lack of highly inflated planets and TESS will find that the occurrence rate of reinflated planets increases sharply as the radii of host stars approach $10\,R_\odot$.

6. Conclusions

In this work, we studied how deposited heating leads to reinflation of hot Jupiters. To do so, we used MESA to compute three suites of planetary evolution models: one to elucidate the process by which planets reinflate, a second studying hot Jupiter evolution with deposited heating over the main-sequence evolution of their host star, and third studying the post-main-sequence reinflation of warm Jupiters. We found that deposited heating can lead to both main-sequence reinflation of hot Jupiters and post-main-sequence reinflation of warm Jupiters, provided it is deep enough and has a sufficient dissipation rate. Our key conclusions are as follows:

1. Deeper heating is required to reinflate planets to a given radius after billions of years of evolution than for the planet to reach the same radius through heating that delays planetary cooling. This is because reinflation must very slowly heat the interior of the planet from the heating level downward and does not greatly affect the central temperature unless the heating is deep. As a result, the radius of a planet after reinflation increases with increasing heating depth and increasing heating rate, with central heating required to lead to maximum reinflation. We compared the analytic theory of Ginzburg & Sari (2015, 2016) for the equilibrium radius and temperature profile of planets that have undergone reinflation to our numerical simulations, finding good agreement throughout the range of heating rates and deposition pressures considered.
2. There is a strong degeneracy between the deposited heating rate and depth that complicates the interpretation of hot Jupiters that are reinflated during the main-sequence evolution of their host stars. As a result, a range of heating profiles can explain the main-sequence reinflation of hot Jupiters, including weak heating of $\approx 0.1\%$ of the incident stellar flux deposited at the very center of the planet and high heating rates of $\gtrsim 1\%$ of the incident stellar flux deposited at a pressure of $\sim 10^3$ bars.
3. The degeneracy between deposited heating rate and depth can be broken in the case of reinflated warm Jupiters orbiting post-main-sequence stars. The radii of recently discovered reinflated warm Jupiters orbiting post-main-sequence stars (Grunblatt et al. 2016, 2017, 2019) can be explained with either weak heating at the center of the planet (Lopez & Fortney 2016) or strong shallow heating. However, post-main-sequence reinflation occurs much more rapidly for deep heating, and shallow heating cannot explain reinflation over late stages of main-sequence host stellar evolution. The large sample of observed reinflated warm Jupiters orbiting post-main-sequence stars that will be obtained by TESS, combined with precise stellar ages, can determine the depth of the heating source that leads to inflation.
4. The dependence of the heating rate on incident stellar flux inferred from the sample of hot Jupiters by Thorngren & Fortney (2018) can explain both main-sequence reinflation of hot Jupiters and post-main-sequence reinflation of warm Jupiters, if heat is deposited at the center of the planet. As a result, the heating rate does not need to have a monotonic dependence on incident stellar flux to lead to reinflation. We find that heating must be weak for warm Jupiters with equilibrium temperatures $\lesssim 1000$ K, as otherwise they would be inflated while their host stars are on the main sequence. The lack of deposited heat in warm Jupiters with $T_{\rm eq} < 1000$ K orbiting main-sequence stars also agrees with the inferred dependence of the deposited heating rate on the incident stellar flux from the hot Jupiter sample. Mechanisms that cause deep heating and decrease in efficacy at low and high incident stellar flux can therefore potentially explain both reinflation of hot Jupiters orbiting main-sequence stars and reinflation of warm Jupiters orbiting post-main-sequence stars.

We thank Jonathan Fortney for insightful comments on an early draft of this manuscript, and we thank Konstantin Batygin and Andrew Youdin for helpful discussions. We thank the referee for thoughtful comments that improved this work. We also thank the MESA team for making this valuable tool publicly available. T.D.K. and S.G. acknowledge support from the 51 Pegasi b Fellowship in Planetary Astronomy sponsored by the Heising-Simons Foundation. D.P.T. acknowledges support by the Trottier Fellowship from the Exoplanet Research Institute (iREx). E.D.L. would like to acknowledge support from the GSFC Sellers Exoplanet Environments Collaboration (SEEC), which is funded in part by the NASA Planetary Science Divisions Internal Scientist Funding Model. This work initiated from discussions at the 2019 Exoplanet Summer Program in the Other Worlds Laboratory (OWL) at the University of California, Santa Cruz, a program funded by the Heising-Simons Foundation. T.D.K. would furthermore like to acknowledge that the bulk of this work was performed on land that is the traditional homeland of the people of the Council of Three Fires, the Ojibwe, Potawatomi, and Odawa as well as the Menominee, Miami, Ho-Chunk, Sac, and Fox nations.

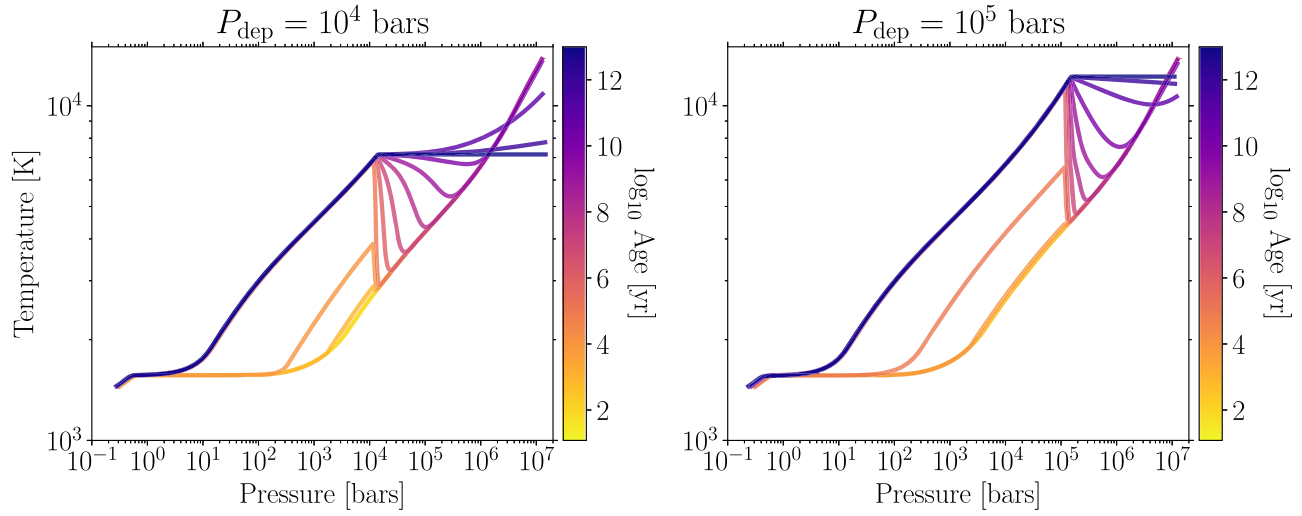

Figure A1. Point-source heat deposition leads to both inside-out and outside-in reinflation. Shown are temperature–pressure profiles at varying ages from 10 to 10^{13} yr for simulations similar to those described in Section 4, with a heating rate of $\gamma = 1\%$ and $P_{\rm dep} = 10^4$ bars (left panel) and $P_{\rm dep} = 10^5$ bars (right panel). However, these experiments use a narrower standard deviation of the heating rate of 0.1 pressure scale heights, rather than the 0.5 used in our standard cases. We use this narrow heating distribution to more accurately reproduce point-source heating and to more cleanly show the effect of heating on inside-out and outside-in reinflation. For visual clarity, we do not identify whether regions are radiative or convective. We find that reinflation from the heating level upward is rapid, occurring in less than a Myr for both cases. As a result, inside-out reinflation occurs much more quickly than outside-in reinflation.

Appendix
Inside-out versus Outside-in Reinflation

To more clearly display the evolution of a planet undergoing reinflation from point-source heat deposition, we consider a narrower heating profile of a Gaussian with a standard deviation of 0.1 pressure scale heights, rather than the 0.5 pressure scale heights used in our nominal grids of simulations. We conducted numerical experiments with this narrowed heating profile for a heating rate of $\gamma = 1\%$ and moderate $P_{\rm dep} = 10^4$ and 10^5 bars, and carried them out to 10 Tyr as in our suite of simulations described in Section 4.

Figure A1 shows the evolution of temperature–pressure profiles from 10 to 10^{13} yr from these two experiments. We find that in both cases, the outer envelope reinflates from the heating level outward. The radiative–convective boundary is deep (at ∼1 kbar) at early times and evolves outward as the planet reinflates. This inside-out heating leads to regions above the heating level becoming convective and reaching a fixed temperature with time by 1 Myr in both cases. Meanwhile, the interior warms up due to deposited heating over much longer timescales, only reaching a fixed isothermal temperature profile below the heating level by 10 Tyr.

The evolution of our cases with point-like heat deposition at early times differs with expectations from the ohmic dissipation models of Wu & Lithwick (2013) and Ginzburg & Sari (2016). In the case of ohmic dissipation alone, reinflation is purely from the heating level downward (i.e., outside in) because the heating rate decays with increasing pressure and because outer regions of the planet have a lower heat capacity than inner regions. However, note that vertical motions could transport deposited heat upward, acting as inside-out heating. For point-source heat deposition, heating acts to reinflate the planet both from the heating level upward (i.e., inside out) and from the outside in. However, the timescale of the inside-out heating is rapid ($\lesssim$1 Myr) relative to the time it takes the planet to reinflate from the outside in, which can be $\gtrsim$1 Tyr for intermediate deposition depths. As a result, the majority of the radius evolution of reinflated planets undergoing point-source heat deposition is determined by the rate of outside-in reinflation.

ORCID iDs

Thaddeus D. Komacek https://orcid.org/0000-0002-9258-5311
Daniel P. Thorngren https://orcid.org/0000-0002-5113-8558
Eric D. Lopez https://orcid.org/0000-0002-7727-4603

References

Arras, P., & Bildsten, L. 2006, ApJ, 650, 394
Arras, P., & Socrates, A. 2010, ApJ, 714, 1
Baraffe, I., Chabrier, G., & Barman, T. 2010, RPPh, 73, 016901
Baraffe, I., Chabrier, G., Fortney, J., & Sotin, C. 2014, in Protostars and Planets VI, ed. H. Beuther et al. (Tucson, AZ: Univ. Arizona Press), 763
Batygin, K., & Stevenson, D. 2010, ApJL, 714, L238
Batygin, K., Stevenson, D., & Bodenheimer, P. 2011, ApJ, 738, 1
Bodenheimer, P., Lin, D., & Mardling, R. 2001, ApJ, 548, 466
Budaj, J., Hubeny, I., & Burrows, A. 2012, A&A, 537, A115
Burrows, A., Hubeny, I., Budaj, J., & Hubbard, W. 2007, ApJ, 661, 502
Chabrier, G., & Baraffe, I. 2007, ApJL, 661, L81
Chandrasekhar, S. 1939, An Introduction to Stellar Structure (Chicago, IL: Univ. Chicago Press)
Choi, J., Dotter, A., Conroy, C., et al. 2016, ApJ, 823, 102
Demory, B., & Seager, S. 2011, ApJS, 197, 12
Dotter, A. 2016, ApJS, 222, 8
Fortney, J., Baraffe, I., & Militzer, B. 2010, in Exoplanets, ed. S. Seager (Tucson, AZ: Univ. Arizona Press), 397
Fortney, J., Marley, M., & Barnes, J. 2007, ApJ, 659, 1661
Fortney, J. J., Lodders, K., Marley, M. S., & Freedman, R. S. 2008, ApJ, 678, 1419
Freedman, R., Marley, M., & Lodders, K. 2008, ApJS, 174, 504
Ginzburg, S., & Sari, R. 2015, ApJ, 803, 111
Ginzburg, S., & Sari, R. 2016, ApJ, 819, 116
Grunblatt, S., Huber, D., Gaidos, E., et al. 2017, AJ, 154, 254
Grunblatt, S., Huber, D., Gaidos, E., et al. 2019, AJ, 158, 227
Grunblatt, S. K., Huber, D., Gaidos, E. J., et al. 2016, AJ, 152, 185
Gu, P., Bodenheimer, P., & Lin, D. 2004, ApJ, 608, 1076
Gu, P., Lin, D., & Bodenheimer, P. 2003, ApJ, 588, 509
Gu, P., Peng, D., & Yen, C. 2019, ApJ, 887, 228
Guillot, T. 2010, A&A, 520, A27
Guillot, T., & Showman, A. 2002, A&A, 385, 156

Hartman, J. D., Bakos, G. Á, Bhatti, W., et al. 2016, AJ, 152, 182
Huang, X., & Cumming, A. 2012, ApJ, 757, 47
Ibgui, L., & Burrows, A. 2009, ApJ, 700, 1921
Ibgui, L., Burrows, A., & Spiegel, D. 2010, ApJ, 713, 751
Jackson, B., Arras, P., Penev, K., Peacock, S., & Marchant, P. 2017, ApJ, 835, 145
Jackson, B., Greenberg, R., & Barnes, R. 2008, ApJ, 681, 1631
Kippenhahn, R., Weigert, A., & Weiss, A. 2012, Stellar Structure and Evolution (2nd ed.; New York: Springer)
Komacek, T., & Showman, A. 2016, ApJ, 821, 16
Komacek, T., Showman, A., & Parmentier, V. 2019, ApJ, 881, 152
Komacek, T., Showman, A., & Tan, X. 2017, ApJ, 835, 198
Komacek, T., & Youdin, A. 2017, ApJ, 844, 94
Kurokawa, Hiroyuki, & Inutsuka, Shu-ichiro 2015, ApJ, 815, 78
Laughlin, G. 2018, The Exoplanet Handbook (Berlin: Springer)
Laughlin, G., Crismani, M., & Adams, F. 2011, ApJL, 729, L7
Laughlin, G., & Lissauer, J. 2015, in Treatise on Geopysics, ed. G. Schubert (2nd ed.; Amsterdam: Elsevier)
Leconte, J., & Chabrier, G. 2012, A&A, 540, A20
Leconte, J., Chabrier, G., Baraffe, I., & Levrard, B. 2010, A&A, 516, A64
Lopez, E., & Fortney, J. 2016, ApJ, 818, 4
Menou, K. 2012, ApJ, 745, 138
Miller, N., & Fortney, J. 2011, ApJL, 736, L29
Miller, N., Fortney, J., & Jackson, B. 2009, ApJ, 702, 1413
Millholland, S. 2019, ApJ, 886, 72
Ohno, K., & Zhang, X. 2019, ApJ, 874, 1
Owen, J., & Wu, Y. 2016, ApJ, 817, 107
Paxton, B., Bildsten, L., Dotter, A., et al. 2011, ApJS, 192, 3
Paxton, B., Cantiello, M., Arras, P., et al. 2013, ApJS, 208, 4
Paxton, B., Marchant, P., Schwab, J., et al. 2015, ApJS, 220, 15
Paxton, B., Schwab, J., Bauer, E., et al. 2018, ApJS, 234, 34
Paxton, B., Smolec, R., Schwab, J., et al. 2019, ApJS, 243, 10
Perez-Becker, D., & Showman, A. 2013, ApJ, 776, 134
Perna, R., Menou, K., & Rauscher, E. 2010, ApJ, 724, 313
Rauscher, E. 2017, ApJ, 846, 69
Rauscher, E., & Menou, K. 2013, ApJ, 764, 103
Rauscher, E., & Showman, A. 2014, ApJ, 784, 160
Rogers, T., & Komacek, T. 2014, ApJ, 794, 132
Rogers, T., & Showman, A. 2014, ApJL, 782, L4
Sainsbury-Martinez, F., Wang, P., Fromang, S., et al. 2019, A&A, 632, A114
Saumon, D., Chabrier, G., & Horn, H. V. 1995, ApJS, 99, 713
Showman, A., & Guillot, T. 2002, A&A, 385, 166
Showman, A., Lewis, N., & Fortney, J. 2015, ApJ, 801, 95
Spiegel, D., & Burrows, A. 2013, ApJ, 772, 76
Thorngren, D., & Fortney, J. 2018, AJ, 155, 214
Thorngren, D., Gao, P., & Fortney, J. 2019, ApJL, 884, L6
Tremblin, P., Chabrier, G., Mayne, N., et al. 2017, ApJ, 843, 30
Valsecchi, F., Rappaport, S., Rasio, F., Marchant, P., & Rogers, L. 2015, ApJ, 813, 101
Weiss, L., Marcy, G., Rowe, J., et al. 2013, ApJ, 768, 14
Wu, Y., & Lithwick, Y. 2013, ApJ, 763, 13
Youdin, A., & Mitchell, J. 2010, ApJ, 721, 1113
Zhang, X., & Showman, A. 2018, ApJ, 866, 2